Magnetic Resonance in Medicine 42:754–761 (1999)

Use of T_2-Weighted Susceptibility Contrast MRI for Mapping the Blood Volume in the Glioma-Bearing Rat Brain

Géraldine Le Duc,[1,4] Michel Péoc'h,[1,2] Chantal Rémy,[1] Odile Charpy,[1] Robert N. Muller,[5] Jean François Le Bas,[1,3] and Michel Décorps[1]*

The aim of this work was to evaluate the potential of T_2-weighted, steady-state susceptibility-enhanced contrast magnetic resonance imaging (MRI), to characterize brain tumor heterogeneity and tumor vascularization. In vivo T_2-weighted MRI experiments were carried out on normal rats (n = 11) and rats bearing C6 glioma (n = 17), before and after the injection of a remanent superparamagnetic contrast agent. The ΔR_2 variations of the transverse relaxation rate due to the injection of the contrast agent were used to generate relative cerebral blood volume (CBV) maps. Contrast enhancement of the tumor was shown to reflect tissue vascularization rather than leakage of the blood-brain barrier. The quantitative results clearly show the heterogeneity of tumor vascularization and reveal a high vessel density in the peripheral area ($CBV_{per} \propto 17.2 \pm 2.3\ sec^{-1}$) and a low vessel density in the central area of the tumor ($CBV_{cen} \propto 2.5 \pm 0.5\ sec^{-1}$). Magn Reson Med 42:754–761, 1999. © **1999 Wiley-Liss, Inc.**

Key words: MRI; nanoparticles; cerebral blood volume; brain tumors

X-ray computed tomography (CT) and MRI have considerably improved the detection and delineation of brain tumors. However, these techniques do not allow the establishment of an etiologic diagnosis (benign or malignant tumors, primary or secondary), which, up to now, has relied on histological analysis of biopsies, a procedure that has several limitations: a) quantitative information about tumor heterogeneity (namely, the proportion of necrotic tissues, viable tumor tissue, and edema) cannot be gained since biopsies sampled small and localized areas (1); b) little information can be obtained about tumor vascularization and blood-brain barrier (BBB) breakdown, which are two important parameters for determining the tumor grade, guiding the therapeutic choices (2–4), and predicting tumor growth (5); c) the invasive character of biopsies restricts the monitoring of tumor growth, especially its evolution from low to high grade. All these limits justify the development of noninvasive techniques capable of improving the characterization of brain tumors and, as a consequence, indicating the choice of appropriate treatment strategies.

The added value of low-molecular-weight contrast agents in the detection and characterization of brain tumors is now well established (6–10). Contrast enhancement arises from leakage of the contrast agent into interstitial space due to BBB breakdown. However, low-molecular-weight contrast agents rapidly diffuse in the interstitium, leading to some blurring of the tumor margins (11). The introduction of T_2^*-sensitive MRI in combination with bolus injection of contrast agents, which produces regional cerebral blood volume (CBV) maps, now provides useful information in addition to that obtained by conventional post-contrast images (2,12–14). However in the case of disrupted BBB, the rapid exchange of tracer from capillaries to interstitial spaces may introduce CBV measurement errors (2). New contrast agents (15–17), such as iron oxide particles, are now available in clinical research and for routine application. Because of the particle size and coating, these contrast agents exhibit a long blood half-life (13,18). Their superparamagnetic properties create susceptibility effects that modify strongly and locally the transverse relaxation rates R_2 and R_2^* (19). Their long half-life in the intravascular pool make steady-state measurements possible. The utility of such steady-state susceptibility contrast MRI methods was recently pointed out (20). An adequate susceptibility effect can be achieved with a smaller injection volume of iron oxide particles than of gadolinium or dysprosium chelates (13). Another potential advantage of iron oxide particles could be to a low leakage rate through a disrupted BBB, on account of their large size. Finally, the information gained from the use of superparamagnetic iron oxide particles for functional characterization of brain tumors could extend beyond the information about tumor vasculature and BBB permeability. Indeed, it was recently shown that iron phagocytosis by glioma cells could be detected in vivo, allowing more accurate delineation of tumor margins (21,22).

The aim of this work was to use an animal model to evaluate the potential of ultrasmall superparamagnetic iron oxide (USPIO) particles, to characterize brain tumor heterogeneity and vascularization. The C6 glioma model was used as a model of high-grade glioblastoma (23). In vivo MRI experiments were carried out on normal and tumorous brain parenchyma of rats, before and after USPIO injection. Since the changes (ΔR_2) in the transverse relaxation rate R_2 due to the contrast agent yields information on microvasculature rather than on macrovasculature (24), all the experiments were carried out by T_2-weighted imaging. Imaging experiments were correlated with histology.

[1]INSERM U438, CHU, BP 217, Grenoble Cédex, France.

[2]Service d'Anatomie Pathologique, CHU, BP 217, Grenoble Cédex, France.

[3]Unité IRM, CHU, BP 217, Grenoble Cédex, France.

[4]European Synchrotron Radiation Facility, BP 220, Grenoble Cédex, France.

[5]Laboratoire de RMN, Département de Chimie Organique, Université de Mons-Hainaut, Mons, Belgique.

Grant sponsors: Laboratoires Guerbet (Aulnay sous Bois, France); INSERM/CFB, Région Rhône-Alpes; Fondation pour la Recherche Médicale; Ligue Nationale Contre le Cancer; Mutuelle Générale de l'Education Nationale; ARC; Grant sponsor: Biomed II project; Grant number: BMH4-CT96-0861.

*Correspondence to: Michel Décorps, INSERM U438, Hôpital Michallon, BP 217, 38043 Grenoble Cédex 9, France. E-mail: Michel.Decorps@ujf-grenoble.fr

Received 18 September 1998; revised 24 June 1999; accepted 25 June 1999.

MATERIALS AND METHODS

Contrast Agent

The USPIO used in this study (Sinerem or AMI-227) was obtained from Laboratoires Guerbet (Aulnay sous Bois, France). In the case of intact BBB, AMI-227 acts as a blood pool contrast agent. In the rat plasma, the half-life is 4.5 hr for a 200 μmole Fe/kg dose and relaxivity values $R_1$and R_2 are, respectively, 23 $sec^{-1} \cdot mM^{-1}$ and 51 $sec^{-1} \cdot mM^{-1}$ at 37°C and 20 MHz (Laboratoires Guerbet, unpublished data). The saturation magnetization of AMI-227 is 0.34 $mT \cdot M^{-1}$ (24). The diameter of the iron oxide core is 4–6 nm (as measured by electron microscopy) and that of the dextran-coated particle is approximately 20 nm (as measured by photon correlation spectroscopy) (13,25).

Experimental Groups

All experiments were carried out on female Sprague-Dawley rats (body weight range 180–220 g). The contrast agent was injected in the saphenous vein at a dose of 200 μmole Fe/kg. The animals were divided into three groups. The control group (group I) consisted of 11 animals and was used to study contrast enhancement in the intact brain. MR images were acquired before and 15 minutes after injection. Rats in group II ($n = 17$) were used for studying contrast enhancement in intracerebral tumor induced by cerebral implantation with C6 glioma cells. The rats were studied by MRI 18 days ($n = 14$), 19 days ($n = 2$), and 20 days ($n = 1$) after tumor implantation. MR images were acquired before and 15 minutes after injection of the contrast agent. In group II, the time-course of the AMI-227 leakage through the BBB was studied in 6 rats out of 17 (18 days after C6 implantation) by performing serial MR imaging during 6 hr after contrast agent injection. Rats in group III ($n = 6$) were used to study the correlation between contrast enhanced MRI and histology. The rats were studied by MRI, before and after injection, 18 ($n = 1$), 22 ($n = 4$), and 23 ($n = 1$) days after C6 cell implantation. The animals were sacrificed less than 12 hr after the MRI experiment, and the brains were sampled for histological examination.

Intracerebral Glioma Model in Rat Brain

Cell Line

The C6 glioma cell line was established by Benda et al. (23) from a methyl nitrosourea-induced rat glioma. Cells were grown in a monolayer with Dulbecco's modified Eagle's medium (DMEM) supplemented with 10% fetal calf serum, 2% L-glutamine, and 0.2% penicillin/streptomycin and incubated at 37°C in a mixture of air/CO_2 (95/5%).

Tumor Implantation

The tumor cells were injected according to a method (26) derived from Kobayashi et al. (27). Before injection in the brain, cells were suspended in a 1% agar solution prepared with supplemented DMEM (10^6 cells/ml). Agarose was used to prevent the spread of cell migration out of the site of injection (26,27). The rats were anesthetized (400 mg/kg of chloralhydrate) and placed on a stereotactic head holder. A middle scalp incision was made. The cell suspension (10^4 cells in 10 μl) was slowly injected (10 sec) using a Hamilton syringe through a burr hole (2.5 mm diameter) in the right caudate nucleus (7.5 mm anterior to the zero ear-bars, 3.5 mm lateral to the midline, 3 mm depth from the dura). The syringe was slowly removed 1 min after the injection. The burr hole was plugged with dental cement and the scalp sutured. Survival time of the rats was about 4–5 weeks after tumor cell implantation. All procedures related to animal care strictly conformed to the Guidelines of the French Government (decree 87–848 of October 19, 1987, licenses 006722 and A38071).

Magnetic Resonance Imaging

Rats were anesthetized with a mixture of halothane and air (0.8 ml/min flow rate). Halothane concentration was 4% to establish the anesthesia, 2% during installation of the rat in the NMR probe, 1% for normal rats, and 0.4–0.8% for rats bearing a glioma during MRI experiment. The body temperature of the rats was kept constant throughout the experiment by using a water-circulated heating blanket. The NMR probe consisted of a nonmagnetic stereotactic head holder and an elliptic surface coil (with semi-major and semi-minor axis 50 and 40 mm, respectively). MRI was carried out on a 40 cm diameter horizontal bore magnet (2.35 T) interfaced to an MSL spectrometer (Bruker Spectrospin, Wissembourg, France) or an SMIS console (Guilford, England). Images of 3 transverse slices and 10 adjacent coronal slices were acquired before and 15 min after injection of the contrast agent. The position of these slices was defined on scout images. The images were acquired using a classical spin-echo (SE) sequence, predominantly T_2-weighted (TE 80 msec, TR 2000 msec). The number of averages for each phase encoding step was 4. The slice thickness was 1 mm. The field of view and bandwidth were respectively 30 mm and 8.33 kHz for normal brain studies and 35 mm and 12.5 kHz for tumor studies. Images were acquired with 64 phase encoding steps, and zero filling was applied to obtain a 128×128 image matrix. With 128 points in the read-out direction, the acquisition time was about 10 msec for tumor studies and 15 msec for normal brain studies. For kinetic studies, six rats were imaged before injection, at 15 min and each hour up to 6 hr post-injection.

Data Analysis

Data analysis was performed on a in-house software using the IDL program operating on a Sun Sparc 10 work station (Sun Microsystems, Mountain View, CA). Signal intensity was determined in several regions of interest (ROI) defined in the normal brain and in the tumor-bearing brain. Signal intensity in each ROI was measured before (I_{before}) and after (I_{after}) contrast agent injection. The results were expressed so as to highlight the changes (ΔR_2) in the relaxation rate due to the injection of the contrast agent. The variation ΔR_2 of the transverse relaxation rate was calculated by using the formula (24):

$$\Delta R_2 = -\frac{\ln(I_{after}/I_{before})}{TE} \quad [1]$$

where TE is the echo time of the imaging sequence, i.e., 80 msec.

In some regions, ΔR_2 was very low. Due to image noise, negative values could be obtained in these regions (in group II, 3 cases out of 17 in the central area of the tumor). In such a case, ΔR_2 has been assume to be zero.

Statistics

Results were expressed as mean ± SEM. The two-sided nonparametric Wilcoxon test was used to compare ΔR_2 differences between different brain areas in the normal or tumor-bearing brains. For the comparison of ΔR_2 changes in one ROI between normal and tumor-bearing brains, a two-sided nonparametric Mann-Whitney test was used. Statistical significance was declared at $P < 0.05$.

Histology

In group III, brains were carefully excised and either frozen in liquid nitrogen vapors or fixed in 10% formalin for 48 hr and embedded in paraffin. Coronal sections of the tumor (3–5 µm) were obtained with either a cryotome or a microtome. Two different staining methods were used: hematoxylin/eosin (HE) and Masson Trichrome (MT).

RESULTS

No deficit nor behavioral or physiological abnormalities were observed during the first 2 weeks after tumor cell implantation. After this period, clinical signs appeared: loss of weight and neurological deficits.

Effect of AMI-227 on the Intact Rat Brain

Figure 1a and b shows T_2-weighted images obtained on healthy rats before and 15 min after AMI-227 injection. AMI-227 induces a marked signal decrease in the whole brain and improves the contrast between gray and white matter. On ΔR_2 maps, large vessels appeared as typical strong hypersignals enhancing their visibility, particularly in the cerebral posterior fossa and meninges (Fig. 1c).

The changes ΔR_2 in the relaxation rate are summarized in Table 1. The cortical areas exhibited the most important modifications. ΔR_2 in the thalamus and caudate putamen were similar, whereas the smallest ΔR_2 changes were measured in the hippocampus and corpus callosum.

Effect of AMI-227 on Experimental Gliomas

Before AMI-227 injection, the tumor appeared as a slight hyperintense area, well-delineated and homogeneous (Fig. 2a). The hyposignal at the center of the tumor is due to agar residue. A mass effect due to the tumor was responsible for a midline shift and a ventricular dilation. Fifteen minutes after AMI-227 injection, the tumor appeared heterogeneous (Fig. 2b). Two areas within the tumor with different patterns could be easily distinguished, the central area (excluding the agar residue) and the periphery.

After injection, the central area of the tumor became markedly hyperintense relative to the contralateral brain. Whereas this area was homogeneous in 10 out of 17 rats, it was punctuated with dark patches in the 7 other rats.

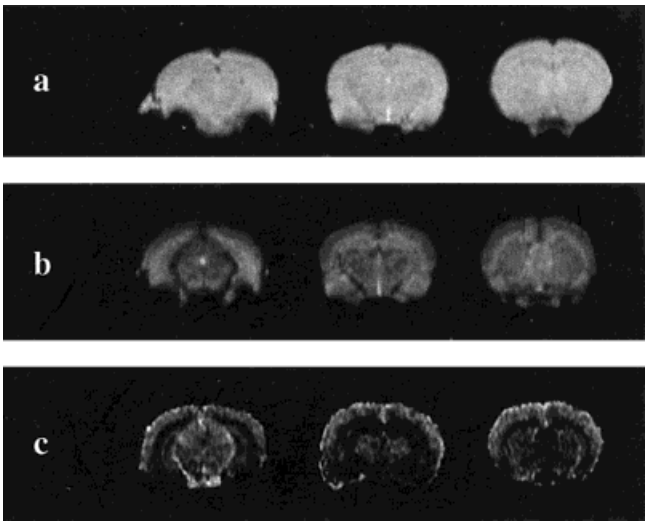

FIG. 1. Coronal MR images (SE, TR/TE 2/0.08 sec) of rat brain before (**a**) and after (**b**) IV administration of AMI-227 (200 µmole Fe/kg) and as a ΔR_2 map (**c**). Note the difference of intensity between gray matter and white matter and also the presence of large vessels in cerebral posterior fossa and meninges.

Analysis of the kinetics of the contrast enhancement revealed further differences. In two out of six rats, the dark patches could not be observed in the central area at any time point. In two other rats, dark patches were not visible on the first images after injection but became visible as time increased after injection. Finally, in the last rats, dark patches could be observed in the central area at any time point, and their size increased as a function of the time.

On the periphery of the tumor, a well-delineated hypointense signal surrounding the central area was always detected. Its thickness varied from slice to slice and rat to rat. Image analysis as a function of time up to 6 hr after injection showed two different patterns (Fig. 3). In some rats (4/6), the thickness and general aspect of the peripheral hypointense ring remained unchanged throughout the 6 hr of follow-up (Fig. 3a). In other rats (2/6), the peripheral

Table 1
ΔR_2 Changes (Mean ± SEM) 15 Minutes After AMI-227 Injection in Normal Brain* and in Brain Bearing a Glioma**

	ΔR_2 (s^{-1})	
Area	Normal brain ($n = 11$)	Brain bearing a glioma ($n = 17$)
Fronto-parietal cortex (cor)	12 ± 0.8	9.4 ± 0.3[a]
Caudate putamen (cau)	9.3 ± 0.5	7.8 ± 0.4[a]
Thalamus (tha)	9.1 ± 0.5	—
Hippocampus (hip)	3.3 ± 0.4	—
Corpus callosum (cal)	2.1 ± 0.4	—
Peripheral area of the tumor	—	17.2 ± 2.3
Central area of the tumor	—	2.5 ± 0.5

*$P < 0.05$ with the nonparametric Wilcoxon test for all data except the difference between caudate putamen and thalamus.
**$P < 0.05$ with the nonparametric Wilcoxon test for all data.
[a]Contralateral hemisphere. The differences between the normal brain and the contralateral area of the brain bearing a glioma were found significant ($P < 0.05$ with non parametric Mann-Whitney test).

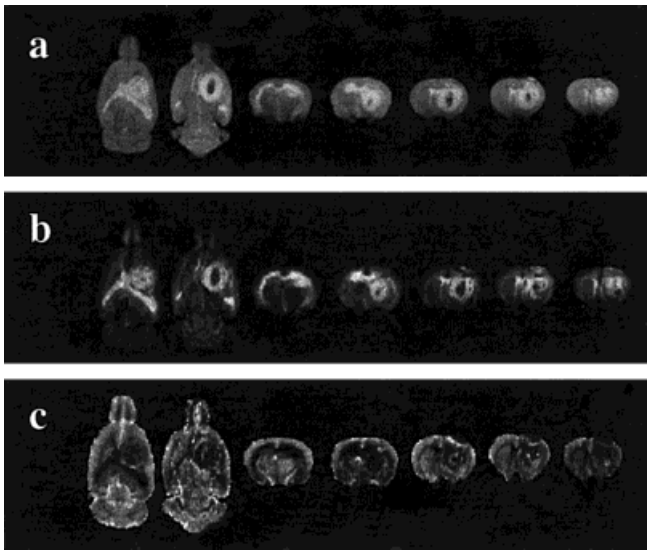

FIG. 2. Coronal and transverse MR images (SE, TR/TE 2/0.08 sec) of rat brain with C6 glioma before (**a**) and 15 min after (**b**) IV administration of AMI-227 (200 μmole Fe/kg) and as a ΔR_2 map (**c**). Note that the hyposignal at the center of the tumor is due to the agar residue.

hypointense ring progressively expanded toward the center of the tumor (Fig. 3b).

Two ROIs were selected in the slice in which the tumor had the largest area. The first ROI was located in the hypointense ring surrounding the tumor, and the second ROI was located in the central area of the tumor. The ΔR_2 changes measured 15 min after injection are summarized in Table 1. The relaxation rate increase (signal decrease) was of much lower magnitude in the central part of the tumor ($\Delta R_2 = 2.5 \pm 0.5$ sec^{-1}, range: 0–5.2) than in the peripheral hypointense ring ($\Delta R_2 = 17.2 \pm 2.3$ sec^{-1}, range: 6.55–44). In the contralateral side, a ROI was located in the fronto-parietal cortex, and another ROI was located in the caudate putamen. The ΔR_2 change in the contralateral fronto-parietal cortex and in the caudate nucleus was equal to 9.4 ± 0.3 and 7.8 ± 0.4 sec^{-1}, respectively (Table 1). Such values are significantly smaller than those measured in the same region in the normal brain ($P < 0.05$).

Figure 4 shows the time course of the normalized change in relaxation rate, $\Delta R_2(t_i)/\Delta R_2(t_0)$, with $t_i = i$ hr ($i = 1$–6) and $t_0 = 15$ min, in the peripheral and in the central areas of the tumor as well as in the contralateral brain, up to 6 hr after injection. In the contralateral brain, ΔR_2 shows a continuing decrease. In contrast, in the peripheral area of the tumor, ΔR_2 shows a gradual increase followed by a gradual decrease. This is less clear in the central part of the tumor.

Comparison of MRI With Histological Findings

The histological examination was undertaken to determine which histological features correspond to the peripheral hypointense ring and the dark patches visible in the images. The tumors (about 5 mm in diameter) invaded the right hemisphere and were fairly limited in their growth without a real capsule. Despite tumor to tumor variability, three clearly distinguishable histological areas could be detected. The central necrotic area presented as a polymorphous shape with vast digitations directed toward the external part of the tumor. The viable tumor area presented as a region of high cellular density containing viable malignant glial cells associated with vasogenous edema. The interstitium was always loose, and the largest extracellular space was about 20 μm. Due to the arrangement of the C6 cells, some pseudo-palisading pattern could be observed around necrotic digitations. The peritumorous area presented as normal tissue with a loose insterstitium due to vasogenic edema. Edema tends to decrease from the tumor to the normal tissue.

The peripheral hypointense signal observed on T_2-weighted images 15 min after injection (Fig. 5b) corresponds clearly on histological sections (Fig. 5c) to a highly vascularized region overlapping the external part of the tumor and the thin area of normal parenchyma surrounding the tumor. Vessel distribution was inhomogeneous, and their lumens were expanded. On the other hand, only a few vessels were found by histology in the necrotic central part of the tumor, whose signal was less affected by AMI-227. The central dark patches seem to correspond to small hemorrhagic foci, visible on histological sections, or to vessels crossing the slice plane.

DISCUSSION

Monitoring relative CBV with MR imaging can be achieved with various techniques. Among them, dynamic suscepti-

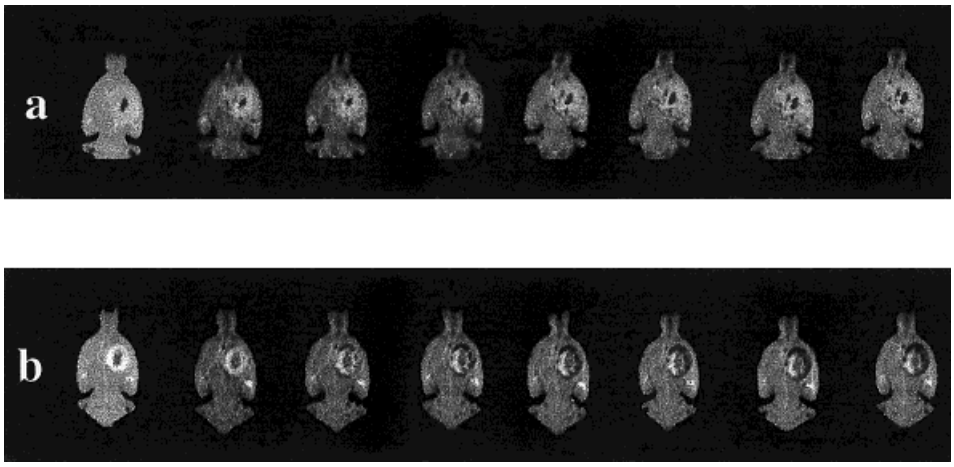

FIG. 3. Transverse MR images (SE, TR/TE 2/0.08 sec) of a kinetic study after a 200 μmole Fe/kg injection to a tumor-bearing rat brain. Note the two different behaviors: either there is no modification (**a**) or the peripheral hypointense ring extended toward the central part of the tumor (**b**).

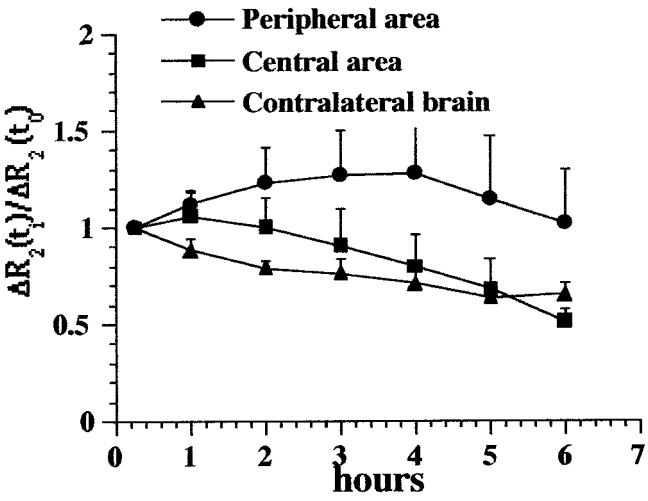

FIG. 4. ΔR_2 changes expressed as a function of time for 3 ROIs in tumorous brain (n = 6/ mean ± SEM): peripheral area of the tumor, central area of the tumor, and contralateral brain. Results were normalized by dividing all values by values obtained 15 min after injection for each rat.

bility imaging using first-pass bolus tracking techniques requires high-speed image acquisition resulting in a relatively low spatial resolution but with the advantage of low doses of tracer. In contrast, steady-state ΔR_2 and ΔR_2^* susceptibility contrast MRI allow high-resolution CBV-weighted images to be obtained at the cost of higher doses of contrast agent.

The potential of superparamagnetic contrast agents for studying microvasculature has been recently pointed out (19,20,24,28–30). It has been shown that, in case of intact BBB, the change ΔR_2 in the transverse relaxation rate is approximately linearly proportional to the average contrast agent concentration in the measured volume and thus to the regional CBV (31). However, the CBV can be expressed as:

$$\mathrm{CBV} = \mathrm{CPV} + \mathrm{CEV} \qquad [2]$$

where CPV is the cerebral plasma volume and CEV the cerebral erythrocyte volume (32–35). In the absence of rupture of the BBB, an MRI contrast agent is a plasma marker. The technique is thus more sensitive to changes in CPV than in CBV. Extrapolation to CBV is based on the assumption that there is no regional variations of hematocrit and that hematocrit remains constant during the experiment. It should be noted that, due to proton exchange, the presence of contrast agent in the vascular bed reduces T_1 in the tissue, resulting in a possible underestimation of ΔR_2. However, due to the use of a long TR, the effects of T_1 changes can be assumed to be small.

In this study, we used a spin-echo rather than a gradient-echo technique. The increase in relaxation rate following the injection of the contrast agent is due to the diffusion of the water protons through the susceptibility gradients induced by the difference $\Delta\chi$ in magnetic susceptibility between the intra- and extra-vascular compartment (24). Compared with gradient echo, spin-echo techniques have a reduced sensitivity: the decrease in the apparent T_2 due to the susceptibility contrast agent is smaller than the decrease in T_2^* (29). However, a spin-echo technique presents the advantage of relative insensitivity to macroscopic susceptibility gradients, which are a source of image artifacts. In particular, a gradient-echo technique is sensitive to both micro- and macro-vasculature whereas a spin-echo technique is mainly sensitive to microvasculature (24,29). It should be noted that T_2^* changes induce changes in k-space weighting: the effective point spread function (PSF) of the spin-echo acquisition is larger after injection. This broadening of the PSF, however, should not modify significantly the mean intensities in volumes of interest (VOIs), whose sizes are generally much greater than the digital resolution.

It has been shown that the change in relaxation rate in a spin-echo experiment depends on the vessel size (24) and displays a peak at a vessel radius that depends on $\Delta\chi$ For $\Delta\chi \approx 0.2$–0.4 ppm, the peak is obtained for capillaries ($R \approx 2.5$ μm). For largest $\Delta\chi$ the peak occurs at a smaller radius than the capillary radius. Under our experimental conditions, $\Delta\chi$ after injection is approximately 0.6 ppm, and the variation of ΔR_2 is expected to be sublinear in $\Delta\chi$ (24). The decay of ΔR_2 with time, in the hemisphere contralateral to

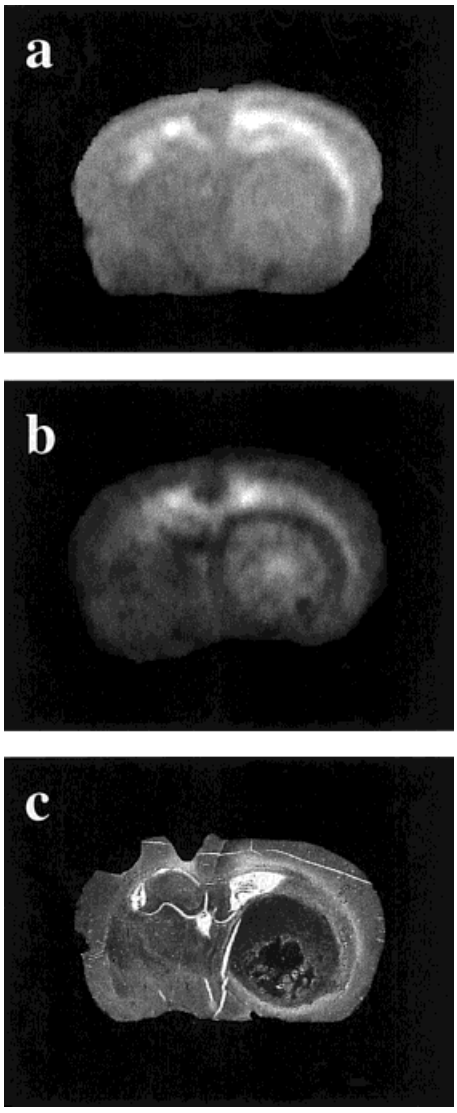

FIG. 5. Correlation among pre-injection image (**a**), post-injection image (**b**), and histological staining (**c**).

the tumor (Fig. 4), is clearly related to clearance of the contrast agent from the vascular compartment. Using the measured half-life in the rat plasma (4.5 hr), the decrease in plasma concentration and thus in $\Delta\chi$ can be calculated at each time point. In Figure 6, ΔR_2 is plotted against $\Delta\chi$. In the range of 0.2 ppm $< \Delta\chi <$ 0.6 ppm, an approximately linear dependence of ΔR_2 on $\Delta\chi$ is observed in the brain hemisphere contralateral to the tumor. However, the curve $\Delta R_2(\Delta\chi)$ shows an offset, suggesting that ΔR_2 is not linearly proportional to $\Delta\chi$ for small $\Delta\chi$ values. For $\Delta\chi$ ppm, the peak of the ΔR_2 vessel size dependence curve occurs at a vessel radius smaller than the capillary radius. For $\Delta\chi$ decreasing from 0 ppm to 0.2 ppm, the maximum of the relaxivity size dependence curve shifts to a larger radius, preventing a decrease of relaxivity proportional to the contrast agent concentration. This effect was theoretically predicted by Boxerman et al. (24). This feature, however, does not prevent CBV measurements: CBV measurements using a steady-state technique require ΔR_2 linearity in blood volume fraction rather than in plasma concentration of agent. Monte Carlo simulations (24) have shown an excellent linearity of ΔR_2 with blood volume fraction in the case of a given distribution of vessel diameter. However, the average vessel diameter can be significantly much larger for the tumor than for the healthy brain tissue. It was recently shown (30) that at given CBV, $1/\Delta R_2$ behaves approximately as the average vessel size. Thus, the use of a spin-echo rather than a gradient-echo technique may result in a significant underestimation of relative CBV in the tumor.

AMI-227 injection induces a large signal intensity decrease in the normal parenchyma. As expected, the ΔR_2 changes depend on the cerebral areas (Table 1). Assuming proportionality between ΔR_2 and CBV, we found $CBV_{cor}/CBV_{cau} = 1.29$, $CBV_{tha}/CBV_{cau} = 0.98$ and $CBV_{hip}/CBV_{cal} = 1.57$. These values agree reasonably well with the data of Bereczki et al. (36): $CBV_{cor}/CBV_{cau} = 1.27$, $CBV_{tha}/CBV_{cau} = 1.09$ and $CBV_{hip}/CBV_{cal} = 1.44$. However, the CBV ratio between highly vascularized brain areas and poorly vascularized brain areas was found to be significantly larger than by autoradiography: $CBV_{cau}/CBV_{cal} = 4.43$, $CBV_{cau}/CBV_{hip} = 2.82$ in this study, $CBV_{cau}/CBV_{cal} = 1.93$, $CBV_{cau}/CBV_{hip} = 1.34$ in Bereczki et al. (36). At this point it should be borne in mind that T_2-weighted CBV measurements are mainly sensitive to capillaries, whereas the autoradiography measurements concern microvessels with diameter smaller than 50 μm (36). The discrepancies between our experimental data and the data of Bereczki et al. (36) might reflect differences in capillary volume fractions. The amount of ΔR_2 increase in the normal brain areas is likely to be correlated to CBV and vascularization. Recently, Jones et al. (29) used a superparamagnetic iron oxide preparation (NSR 043, saturation magnetization: 0.52 mT · M_{-1}, dose: 60 μM Fe/kg) to study CBV with a spin-echo sequence in a rat model of acute focal cerebral ischemia. In the brain contralateral to the focal ischemia, they found $\Delta R_2 \approx 4.7$ sec^{-1} in the frontal parietal cortex and $\Delta R_2 \approx 3.6$ sec^{-1} in the caudate putamen. These values can be compared with the results of the present study: $\Delta R_2 \approx 12$ sec^{-1} in the frontal parietal cortex and $\Delta R_2 \approx 9.3$ sec^{-1} in the caudate putamen. First, the ratio $CBV_{cor}/CBV_{cau} = 1.30$ found by Jones et al. (29) is close to the ratio $CBV_{cor}/CBV_{cau} = 1.29$ obtained in the present study. Second, assuming that ΔR_2 depends linearly on both dose (200 μmole Fe/kg vs 60 μM Fe/kg) and tracer magnetization (0.34 mT · M^{-1} vs 0.52 mT · M^{-1}), the ΔR_2 changes reported in this work can be compared with the results of Jones et al. (29). The results found in the present study would yield under the conditions used by Jones et al. (29), $\Delta R_2 \approx 5.49$ sec^{-1} in the frontal parietal cortex and $\Delta R_2 \approx 4.27$ sec^{-1} in the caudate putamen, which are in reasonable agreement with the results of Jones et al. (29) (4.7 sec^{-1} and 3.6 sec^{-1}, respectively).

In the contralateral hemisphere of rats bearing an intracerebral tumor, ΔR_2 was found to be smaller than in the normal brain. The difference is statistically significant ($P = 0.05$) in the cortex (9.4 ± 0.3 sec^{-1} vs 12 ± 0.5 se^{-1} in the normal brain) and in the caudate putamen (7.8 ± 0.4 sec^{-1} vs 9.3 ± 0.5 sec^{-1} in the normal brain). This reduction in CBV will be associated with compression of the contralateral hemisphere, which is demonstrated by the shift of the midline.

The proportionality between ΔR_2 and CBV relies on the assumption that the permeability of the BBB to the contrast agent is very low. In the tumor, the kinetic study yields evidence of BBB permeability to the contrast agent: a) the dark patches, if present, increase in size with time after injection; b) the peripheral hypointense ring progressively expands toward the tumor center in two of six rats (Fig. 3); and c) ΔR_2 in this ring slowly increases with time (Fig. 4). Leakage of the contrast agent into the extra-vascular space produces a change both in the susceptibility difference between extra- and intra-vascular spaces and in T_1 and T_2 due to the direct interaction of extravascular water molecules with the contrast agent. However, the inaccuracy in blood volume measurement introduced by the leakage of the contrast agent into the interstitial space should be small if the transport from intra-vascular to extra-vascular space is slow. Information on the amount of initial leakage into the extra-vascular space may be obtained by comparing the enhancement kinetics in the normal contralateral brain and in the tumor. The ΔR_2 time-course shows a slow increase followed by a decrease in the tumor periphery and a continuous decay in the contralateral brain (Fig. 4). In the central area of the tumor ΔR_2 remains constant during the first 2 hr after injection and then decreases. These results

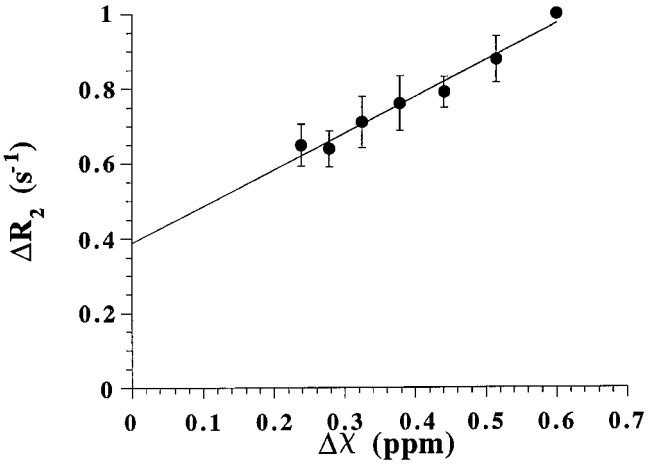

FIG. 6. ΔR_2 changes plotted against $\Delta\chi$.

suggest a leakage of the contrast agent into the interstitial space in the tumor. Due to its large size (20 nm), the transport of the contrast agent across the blood vessel walls as well as the subsequent diffusion in the interstitium is probably very slow. As time after injection increases, the contrast agent particles leaving the vascular space slowly diffuse within the interstitium, increasing progressively the apparent size of the compartment containing the contrast agent, which results in an increase in ΔR_2 and in a decrease in T_1. Both phenomena increase the ratio $I_{\text{after}}/I_{\text{beforee}}$. As time increases, the concentration gradient, and thus the susceptibility gradient, around the capillaries decrease. The decrease in ΔR_2, which follows the peak might be due to the progressive decrease of these susceptibility gradients, which are at the origin of the changes in the relaxation rate R_2. From the data of Fig. 4, the initial slope of the curve $\Delta R_2(t_i)/\Delta R_2(t_0)$ was found to be equal to $\approx$ 0.02 hr^{-1} in the central area and $\approx$ 0.12 hr^{-1} in the periphery. Thus in both cases, 15 min after injection, the changes in ΔR_2 due to the leakage of the contrast agent into the interstitial space are probably much smaller than the initial relaxation rate changes induced by the contrast agent injection. Therefore, as expected, contrast enhancement obtained within 15 min after AMI-227 injection reflects the tumor micro-vascularization rather than leakage of the BBB. Thus, due to the large size of the agent, the error introduced by the permeability of the BBB can be assumed to be low.

The quantitative results (Table 1) clearly show the heterogeneity of tumor vascularization and reveal a high vessel density in the peripheral area ($CBV_{per} \propto 17.2 \pm 2.3$ sec^{-1}) and a low vessel density in the central area of the tumor ($CBV_{cen} \propto 2.5 \pm 0.5$ sec^{-1}). By comparing these results with those obtained in the contralateral hemisphere, one can obtain $CBV_{per}/CBV_{cor} = 1.83$, and $CBV_{cen}/CBV_{cor} = 0.26$. Given that CBV measurement in the tumor with a spin-echo technique may be underestimated if the mean vessel size is, as expected, larger than in normal brain, we conclude that the tumor peripheral area is more vascularized than the normal cortex. In contrast, CBV is smaller in the central area of the tumor than in the normal cortex. Comparison of MRI with histology further supports these findings. It should be noted, however, that the contrast agent-enhanced MRI highlights only functional vessels whereas histology exhibits all kinds of endothelial cells of both functional and nonfunctional vessels.

Compared with AMI-227, the transport of gadolinium (Gd) chelates through the BBB and their diffusion into the interstitium are much more rapid, resulting in a very small time to peak and in an underestimation (2) of the blood volume measured with dynamic susceptibility-weighted imaging. This difference of behaviors is related to the small size of Gd chelates (around 1 nm) compared with AMI-227 (20 nm). Fifteen minutes after AMI-227 injection, contrast enhancement is visible only in the highly vascularized regions of the tumor. Later on, two different patterns were observed (Fig. 3). The expansion of the peripheral hypointense ring toward the center of the tumor observed in some rats (2/6), could be explained by a slow extravasation and diffusion of AMI-227 into the interstitial space of the tumor, which, at late stage of tumor growth, is quite large. Due to its large size compared with Gd chelates, the USPIO particles might hardly diffuse into the interstitial space of normal tissue. In addition, it has been shown that exposure of glioma tumors to an iron oxide preparation leads to phagocytic uptake by tumoral cells (21,22). T_2-weighted MRI performed 12 or 24 hr after injection (21) showed a hypointense ring corresponding to the area of viable tumor cells quite similar to that reported in the present paper. Thus, the expansion of the peripheral hypointense ring could be due to the slow extravasation and diffusion of AMI-227 into interstitial space and phagocytic uptake by C6 cells. In the other rats (4/6), the peripheral hypointense ring did not expand toward the center of the tumor during 6 hr after injection. However, ΔR_2 remained constant or continued to increase with time. These results suggest that the BBB is permeable to AMI-227 but that the contrast agent diffuses extremely slowly in a tight tumor interstitium. This pattern might occur at earlier stages of tumor growth. However, testing these hypotheses requires further experiments since no quantitative correlation between MRI and histology was performed. Nevertheless these findings show that kinetic studies could give information about BBB permeability and tumor architecture or organization.

CONCLUSIONS

We have shown that T_2-weighted steady-state susceptibility contrast MRI can be used for studying intracerebral tumor vascularization. The method offers a higher spatial resolution and sensitivity than bolus tracking techniques. Compared with T_2^*-weighted steady-state susceptibility contrast MRI, the method is mainly sensitive to microvasculature and is relatively free of detrimental artifacts due to boundaries between macroscopic regions of different susceptibility. In the normal brain we have shown that relative CBV estimates agree reasonably well with quantitative autoradiography (32). In the tumor we found that the BBB permeability to the USPIO contrast agent was small, allowing blood volume estimate undisturbed by leakage into the interstitial space. We have shown that MRI microvasculature characterization correlates with histology, suggesting that the method could be of interest to improve characterization of brain tumor vascularization. It is generally well recognized that increased malignancy is associated with increased vascularization and that the acceleration of the tumor growth is correlated with the angiogenesis phenomenon (4,5,14,15,37,38). Thus, the use of contrast agents with high molecular weight can be interesting for clinical cerebral imaging to grade in vivo brain tumors, to choose the appropriate therapy, and to follow up the tumor evolution. Furthermore, CBV imaging could be useful to determine the transition time from tumor dormancy (low grade) to tumor aggressiveness (high grade) and to assess tumor heterogeneity.

ACKNOWLEDGMENTS

We thank Marie France Nissou (INSERM U318), Régine Farion, and Olivier Montigon (INSERM U438), and Denise Noel and Evelyne Sage (Service d'Anatomie Pathologique) for technical assistance. We also thank Soraya Benderbous

(Laboratoires Guerbet) and Ralph Weissleder (Massachusetts General Hospital) for helpful discussions.

REFERENCES

1. Burger PC, Kleihues P. Cytologic composition of the untreated glioblastoma with implication for evaluation of needle biopsies. Cancer 1989;63: 2014–2023.
2. Aronen HJ, Gazit IE, Louis DN, Buchbinder BR, Pardo FS, Weisskoff RM, Harsh GR, Cosgrove GR, Halpern EF, Hochberg FH, Rosen BR. Cerebral blood volume maps of gliomas: comparison with tumor grade and histological findings. Radiolody 1994;191:41–51.
3. Sage MR, Wilson AJ. The blood brain barrier: an important concept in neuro-imaging. AJNR 1994;15:601–622.
4. Abramovitch R, Meir G, Neeman M. Neovascularization induced growth of implanted C6 glioma multicellular spheroids: magnetic resonance micro-imaging. Cancer Res 1995;55:1956–1962.
5. Folkman J. Angiogenesis in cancer, vascular, rheumatoid and other diseases. Nature Med 1995;1:27–31.
6. Brant-Zawadski M, Berry I, Osaki L, Brasch R, Murovic J, Norman D. Gd-DTPA in clinical MR of the brain. AJNR 1986;7:781–788.
7. Bronen RA, Szende G. Magnetic resonance imaging contrast agents: theory and application to the central nervous system. J Neurosurg 1990;73:820–839.
8. Kenney J, Schmiedl U, Maravilla K, Starr F, Graham M, Spence A, Nelson J. Measurement of blood brain barrier permeability in a tumor model using magnetic resonance imaging with gadolinium-DTPA. Magn Reson Med 1992;27:68–75.
9. Krueck WG, Schmiedl UP, Maravilla KR, Spence AM, Starr FL, Kenney J. MR assessment of radiation-induced blood brain permeability changes in a rat glioma model. AJNR 1994;15:625–632.
10. Kurki T, Komu M. Spin-lattice relaxation and magnetization transfer in intracranial tumors in vivo: effects of Gd-DTPA on relaxation parameters. Magn Reson Imaging 1995;13:379–385.
11. Yuh WTC, Nguyen HD, Tali ET, Mayr NA, Fischer DJ, Atlas SW, Carvlin MC, Drayer BP, Pollei SR, Runge VM, Sze GK. Delineation of gliomas with various doses of MR contrast material. AJNR 1993;15:983–989.
12. Rempp KA, Brix G, Wenz F, Becker CR, Gückel F, Lorenz WJ. Quantification of regional cerebral blood flow and volume with dynamic susceptibility contrast-enhanced MR imaging. Radiology 1994;193:637–641.
13. Unger EC, Ugurbil K, Latchaw RE. Contrast agents for cerebral perfusion MR imaging. J Magn Reson Imaging 1994;4:235–242.
14. Maeda M, Itoh S, Kimura H, Iwasaki T, Hayashi N, Yamamoto K, Ishii Y, Kubota T. Tumor vascularity in the brain: evaluation with dynamic susceptibility contrast MR imaging. Radiology 1993;189:233–238.
15. Tiefenauer LX, Tschirky A, Kühne G, Andres RY. In vivo evaluation of magnetite nanoparticles for use as a tumor contrast agent in MRI. Magn Reson Imaging 1996;14:391–402.
16. Brasch RC. New directions in the development of MR imaging contrast media. Radiology 1992;183:1–11.
17. Saini S, Frankel RB, Stark D, Ferrucci J. Magnetism: a primer and review. AJR 1987;150:735–743.
18. Weissleder R, Elizondo G, Wittenberg J, Rabito CA, Bengele HH, Josephson L. Ultrasmall superparamagnetic iron oxide: characterization of a new class of contrast agent for MR imaging. Radiology 1990;175:489–493.
19. Villringer A, Rosen BR, Belliveau JW, Ackermann JL, Lauffer RB, Buxton RB, Chao YS, Wedeen VJ, Brady TJ. Dynamic imaging with lanthanide chelates in normal brain: contrast due to magnetic susceptibility effects. Magn Reson Med 1998;6:164–174.
20. Hamberg LM, Boccalini P, Stranjalis G, Hunter GJ, Huang Z, Halpern E, Weisskoff RM, Moskowitz MA, Rosen BR. Continuous assessment of relative cerebral blood volume in transient ischemia using steady state susceptibility-contrast MRI. Magn Reson Med 1996;35:168–173.
21. Zimmer C, Weissleder R, Poss K, Bogdanova A, Wright SC, Enochs WS. MR imaging of phagocytosis in experimental gliomas. Radiology 1995; 197:533–538.
22. Zimmer C, Wright SC, Engelhardt RT, Johnson GA, Kramm C, Breakefield XO, Weissleder R. Tumor cell endocytosis imaging facilitates delineation of the glioma brain interface. Exp Neurol 1997;143:61–69.
23. Benda P, Someda K, Messer J, Sweet W. Morphological and immunochemical studies of rat glial cells in tumors and clonal strains propagated in tissue culture. J Neurosurg 1971;34:310–323.
24. Boxerman JL, Hamberg LN, Rosen BR, Weisskoff R. MR contrast due to intravascular magnetic susceptibility perturbations. Magn Reson Med 1995;34:555–566.
25. Chambon C, Clement O, Le Blanche A, Schouman-Claeys E, Frija G. Superparamagnetic iron oxides as positive M.R. contrast agents: in vitro and in vivo evidence. Magn Reson Imaging 1993;11:509–519.
26. Benabid AL, Remy C, Chauvin C. Experimental model of rat brain tumors by stereotactic injection of C6 glioma and HTC hepatoma cell lines. In: Walker MD, Thomas DGT, editors. Biology of brain tumors. Amsterdam: Martinus Nijhoff Publishers; 1986. p 221–226.
27. Kobayashi N, Allen N, Clendenon NR, Ko LW. An improved rat brain-tumor model. J Neurosurg 1980;53:808–815.
28. Fisel CR, Ackerman JL, Buxton RB, Garrido L, Belliveau JW, Rosen BR, Brady TJ. MR contrast due to microscopically heterogeneous magnetic susceptibility: numerical simulations and applications to cerebral physiology. Magn Reson Med 1991;17:336–347.
29. Jones RA, Haraldseth O, Baptista AM, Müller TB, Øksendal AN. A study of the contribution of changes in the cerebral blood volume to the haemodynamic response to anoxia in rat brain. NMR Biomed 1997;10: 59–66.
30. Dennie J, Mandeville JB, Boxerman JL, Packard SC, Rosen BR, Weisskoff RM. NMR imaging of changes in vascular morphology due to tumor angiogenesis. Magn Reson Med 1998;40:793–799.
31. Payen JF, Väth A, Koenigsberg B, Bourlier V, Décorps M. Regional cerebral plasma volume response to CO2 using magnetic resonance imaging. Anesthesiology 1998;88:984–992.
32. Bereczki D, Wei L, Otsuka T, Acuff V, Pettigrew K, Patlak C, Fenstermacher J. Hypercapnia slightly raises blood volume and sizably elevates flow velocity in brain microvessels. Am J Physiol 1993;264:1360–1369.
33. Keyeux A, Ochrymowicz-Bemelmans D, Charlier AA. Induced response to hypercapnia in the two-compartment total cerebral blood volume: influence on brain vascular reserve and flow efficiency. J Cereb Blood Flow Metab 1995;15:1121–1131.
34. Sakai F, Nakazawa K, Tazaki Y, Ishii K, Hino H, Igarashi H, Kanda T. Regional CBV and hematocrit measured in normal human volunteers by single-photon emission computed tomography. J Cereb Blood Flow Metab 1985;5:207–213.
35. Berry I, Benderbous S, Ranjeva JP, Gracia-Méavilla D, Manelfe C, Le Bihan D. Contribution of Sinerem used as a blood-pool contrast agent: detection of cerebral blood volume changes during apnea in the rabbit. Magn Reson Med 1996;36:415–419.
36. Bereczki D, Wei L, Otsuka T, Acuff V, Pettigrew K, Patlak C, Fenstermacher J. Hypoxia increases velocity of blood flow through microvascular systems in rat brain. J Cereb Blood Flow Metab 1993;13:475–486.
37. Nagano N, Sasaki H, Aoyagi M, Hirakawa K. Invasion of experimental rat brain tumor: early morphological changes following micro-injection of C6 glioma. Acta Neuropathol 1983;86:117–125.
38. Passe TJ, Bluemke DA, Siegelman SS. Tumor angiogenesis: tutorial on implications for imaging. Radiology 1997;203:593–560.